Comparison of zonal neutral winds with equatorial plasma bubble and plasma drift velocities

Narayan P. Chapagain,[1] Daniel J. Fisher,[1] John W. Meriwether,[2] Jorge L. Chau,[3] and Jonathan J. Makela[1]

Received 16 October 2012; revised 5 February 2013; accepted 15 March 2013; published 25 April 2013.

[1] A one-year dataset spanning March 2011 to March 2012 of coincident observations of nighttime thermospheric zonal neutral winds, equatorial plasma bubble (EPB) velocities, and zonal plasma drifts is used to examine the relationship between the thermosphere and the ionosphere near the geomagnetic equator over Peru. Thermospheric neutral winds are determined by using a bistatic Fabry-Perot interferometer (FPI) experiment located at Merihill and Nazca in Peru. The ambient plasma drift velocities were obtained using the incoherent scatter radar at the Jicamarca Radio Observatory in Peru. The EPB zonal velocities were estimated utilizing images of the OI 630.0 nm emission recorded by a narrow-field optical imaging system at the Cerro Tololo Inter-American Observatory in Chile. The joint analysis of these datasets illustrates that the nighttime and night-to-night variations in the zonal neutral winds, EPB velocities, and plasma drifts are well correlated. This consistent result of the local time variations of the neutral winds with that of EPB and plasma drifts illustrates that the *F*-region dynamo is, in general, fully activated. However, at times, the magnitude of the EPB velocities and the plasma drifts are different from the neutral winds. It is plausible that such a difference is due either to the effect of polarization electric fields developed inside the EPB or due to the latitudinal gradient of the neutral winds and EPB velocity measurements since the EPB velocities are estimated at a higher latitude, corresponding to an apex altitude of ~400 km, than the wind estimates, which derive from an apex altitude of ~250 km.

Citation: Chapagain, N. P., D. J. Fisher, J. W. Meriwether, J. L. Chau, and J. J. Makela (2013), Comparison of zonal neutral winds with equatorial plasma bubble and plasma drift velocities, *J. Geophys. Res. Space Physics*, *118*, 1802–1812, doi:10.1002/jgra.50238.

1. Introduction

[2] In the evening sector, the horizontal pressure gradient across the terminator produces large thermospheric eastward zonal neutral winds which are important to thermospheric and ionospheric dynamics through the development of the *F*-region dynamo [e.g., *Rishbeth*, 1971; *Heelis et al.*, 1974; *Kelley*, 1989]. Several studies have documented the zonal neutral winds using ground-based Fabry-Perot interferometer (FPI) measurements [e.g., *Meriwether et al.*, 1986; 2011; *Biondi et al.*, 1991; *Martinis et al.*, 2001; Makela *et al.*, 2013] and satellite-based observations [e.g., *Wharton et al.*, 1984; *Liu et al.*, 2009]. Similarly, the low-latitude zonal plasma drifts in the *F*-region have been extensively studied over the past few decades using a variety of ground- and satellite-based observations [e.g., *Woodman*, 1972; *Valladares et al.*, 1996; *Kudeki and Bhattacharyya*, 1999; *Kelley et al.*, 2003; *Immel et al.* 2004; *Fejer et al.*, 2005].

[3] *Woodman* [1972] first described the characteristics of the equatorial *F*-region zonal plasma drift, and since then, extensive studies have been performed using the Jicamarca incoherent scatter radar (ISR) [e.g., *Fejer et al.*, 1985; 2005]. Furthermore, optical observations of the nighttime *F*-region equatorial ionosphere have been conducted from various low-latitude sites to study large-scale ionospheric depletions, or equatorial plasma bubbles (EPBs), and their zonal drift velocities [e.g., *Mendillo and Baumgardner*, 1982; *Martinis et al.*, 2003; *Yao and Makela*, 2007; *Sobral et al.*, 2009; *Chapagain et al.*, 2011].

[4] The study of the coupling relationship between the zonal neutral winds and the *F*-region plasma drifts is important for gaining an understanding of the dynamics and structures of the thermosphere and ionosphere at low latitudes. The equatorial zonal neutral winds flowing across the Earth's magnetic field during the post-sunset period impart a slow transverse drift to the ions perpendicular to both the wind and the

[1]Department of Electrical and Computer Engineering, University of Illinois at Urbana-Champaign, Urbana, Illinois, USA.
[2]Department of Physics and Astronomy, Clemson University, Clemson, South Carolina, USA.
[3]Radio Observatorio de Jicamarca, Instituto Geofisico del Peru, Lima, Peru.

Corresponding author: N. P. Chapagain, Department of Electrical and Computer Engineering, University of Illinois at Urbana-Champaign, Urbana, IL 61801, USA. (chapagai@illinois.edu)

2169-9380/13/10.1002/jgra.50238

geomagnetic field resulting in a vertical polarized electric field [*Rishbeth*, 1971]. At night, due to the lower conductivity of the *E*-region, the polarization electric field builds up in the *F*-layer, which causes the plasma to move eastwards in the direction of the wind flow. As the nighttime *E*-region plasma densities rapidly decay and the *E*-region dynamo becomes negligible, the *F*-region dynamo dominates the nighttime plasma drifts [e.g., *Coley and Heelis*, 1989]. Under such conditions, the neutral and ionized portions of the atmosphere at *F*-region altitudes move eastward at the same speed.

[5] Several previous studies have been carried out investigating coincident measurements of low-latitude *F*-region neutral winds and plasma drifts or EPB/scintillation drift velocities [e.g., *Biondi et al*. 1988; *Basu et al*., 1991; 1996; *Valladares et al*., 2002; *Chapagain et al*., 2012a]. *Biondi et al*. [1988] compared Fabry-Perot interferometer (FPI) derived neutral winds and the ISR ion drift velocity from Jicamarca using 2 days of simultaneous data and found correlated motions of the neutrals and the ionospheric plasma drifts. *Basu et al*. [1991] presented simultaneous observations of zonal irregularity drift velocities obtained from both spaced-receiver scintillation and radar techniques at Huancayo, Peru, and zonal neutral winds from an FPI at Arequipa from a 3 day campaign and suggested that the neutral winds sometimes exceeded the irregularity drifts by a factor of 2. Further, *Basu et al*. [1996] compared scintillation drift measurements from Ancon, Peru, to the Arequipa FPI measurements of neutral winds and noted that the day-to-day variability of the zonal thermospheric winds might potentially explain the day-to-day variability of ESF development. Each of these studies was carried out over a short period, and thus, the resultant conclusion regarding the correlative relationship between the zonal neutral winds and plasma or scintillation drifts was drawn from a limited data set. Additional correlations between the neutral winds and scintillation drifts from an extended data set from the Peruvian region have been reported by *Valladares et al*. [2002] and indicated that the relative velocities between winds and drift values vary depending on season and solar activity.

[6] Other studies have reported similar local time variations of plasma drift velocities and neutral winds [e.g., *Rishbeth*, 1971; *Heelis et al*., 1974; *Fejer et al*. 1985; *Martinis el al*., 2001]. *Fejer et al*. [1985] demonstrated that the average zonal plasma drift velocity obtained from the Jicamarca ISR was in good agreement with the zonal neutral wind observed by the DE-2 satellite reported by *Wharton et al*. [1984]. Recently, *Chapagain et al*. [2012a] presented results from a 5 month dataset of coincident measurements of EPB velocities using an all-sky imaging system and thermospheric neutral wind derived from FPIs operating in Brazil. They reported that the *F*-region dynamo is not fully activated in the early evening hours. However, after ~22:00 LT, they showed consistent results between the neutral wind and EPB velocity illustrating that the *F*-region dynamo is nearly fully activated.

[7] Many of the previous studies near the equatorial region have suffered from a lack of an extensive database of simultaneous measurements of ambient plasma drifts or plasma depletions and neutral dynamics. In this paper, we present the results of 12 months (March 2011 through March 2012) of coincident nighttime zonal neutral winds measurements obtained from a bistatic FPI system near the geomagnetic equator in Peru, measurements of equatorial plasma bubble (EPB) drift velocities from the optical signature of the OI 630.0 nm nightglow emission from the Cerro Tololo Inter-American Observatory (CTIO), Chile, along approximately the same geomagnetic meridian as the neutral winds measurements, and measurements of the ambient zonal plasma drift velocities obtained from the incoherent scatter radar (ISR) facility at the Jicamarca Radio Observatory (JRO) in Peru.

2. Experiments and Measurement Techniques

[8] The database used in this study was derived from a bistatic FPI system operated at Merihill (geographic: 11.96°S, 76.86°W; geomagnetic: 0.57°N, 5.13°W) and Nazca (geographic: 14.97°S, 74.89°W; geomagnetic: 4.16°S, 2.52°W) in Peru, ISR observations obtained at the Jicamarca Radio Observatory (geographic: 11.95°S, 76.87°W; geomagnetic: 0.58°N, 5.12°W) in Peru, and a Portable Ionospheric Camera and Small-Scale Observatory (PICASSO) narrow-field optical imaging system located at the Cerro Tololo Inter-American Observatory (geographic: 30.17°S, 70.81°W; geomagnetic: 16.72°S, 0.42°E) in Chile. The FPI system is used to measure the neutral winds for studying background thermospheric conditions, the collocated Jicamarca ISR measurements are used to derive the equatorial *F*-region zonal plasma drifts, and the observations from the PICASSO imager record the two-dimensional spatial and temporal properties of the ionospheric depletion structures used to derive EPB velocities. The distribution of the instrumentation sites used in this study is shown in Figure 1. The sites are represented as "JRO" for Jicamarca Radio Observatory, "MRH" for Merihill, "NZK" for Nazca, and "CTIO" for the Cerro Tololo Inter-American Observatory. The points "CVE" and "CVW" are the locations of the common volume mode observations in east and west look directions, respectively, whereas the "East" marker denotes the east look direction from Merihill used for the wind measurements, as described below.

2.1. Wind Measurements

[9] The neutral wind measurements reported in this study were obtained from FPI instruments deployed at Merihill and Nazca in Peru near the geomagnetic equator (as shown in Figure 1). The two FPI sites are separated by ~395 km allowing the individual instruments to measure orthogonal line-of-sight Doppler speeds in a common thermospheric volume. These measurements can be combined to infer the vector horizontal neutral wind at the common volume location without making assumptions about the uniformity of the wind field. The details of the analysis methods of the FPI measurements have been described in previous studies [*Makela et al*., 2011; *Meriwether et al*., 2011; *Chapagain et al*., 2012a] and is briefly discussed below.

[10] The FPIs at both Merihill and Nazca consist of a 70 mm diameter etalon with a reflectivity of ~77% at 630.0 nm having a fixed air gap of 1.5 cm. The etalons are thermally controlled within ±0.1°C at 30°C. To isolate the emission of interest, a 77 mm diameter interference filter centered at 630.0 nm is placed in front of the etalon. The filter has a full-width half maximum of ~0.8 nm and a peak

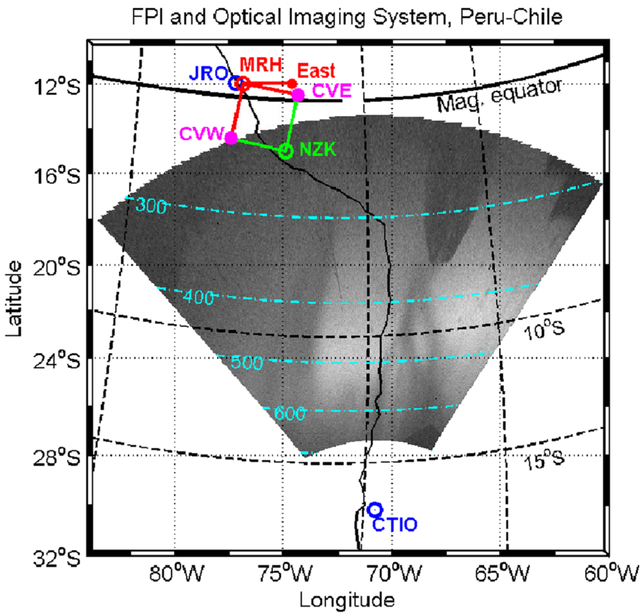

Figure 1. Map showing the distribution of the observation sites from Peru and Chile as indicated as MRH (Merihill), NZK (Nazca), JRO (Jicamarca Radio Observatory), CVE and CVW (common volume mode at east and west look directions), East (east look direction from Merihill), and CTIO for PICASSO imager. The dark region represents the field of view of the imager mapped to an assumed altitude of 250 km, and the dash-dotted lines (cyan color) correspond to the apex altitudes whereas the dashed lines (black color) in the map indicate geomagnetic latitudes.

transmission of ~60%. The FPI at Merihill uses a 35 cm focal length lens to image approximately eight rings of the interference pattern onto an Andor Technology DU-434 CCD camera. At Nazca, a 31 cm focal length lens images ~11 rings of the interference pattern onto an Andor Technology Class iKon DU-934 CCD camera. Both cameras use a 1024 × 1024 pixel CCD chip, with each square pixel having a dimension of 13.0 μm × 13.0 μm. The CCD is cooled down to at least −60°C to reduce the effects of dark noise on the imaged interference patterns.

[11] The Doppler shifts in the observed 630.0 nm interference image pattern are used to estimate the nighttime thermospheric winds. The OI 630.0 nm nightglow emission is created from the dissociative recombination of O_2^+ to $O + O(^1D)$ [*Link and Cogger*, 1988] with a peak emission altitude assumed to be ~250 km. To obtain the measurement of the line-of-sight Doppler shift in a desired look direction, a dual mirror sky-scanning system is used that has a pointing accuracy of ~0.2°. The exposure time is 240 s for each 630.0 nm image.

[12] As discussed by *Makela et al*. [2011], each image contains multiple orders of the 630.0 nm emission spectra collected by the instrument. Each order is analyzed individually to extract the estimates of Doppler shift (neutral wind), Doppler broadening (neutral temperature), 630.0 nm intensity, and background continuum intensity. The individual estimates obtained from each order are averaged together, weighted by the uncertainty of the individual estimates, to obtain the final estimated parameters used here. A zero reference for the Doppler shifts must be established to obtain absolute estimates of the line-of-sight neutral wind. For this study, we use observations of a frequency-stabilized HeNe laser as our absolute reference. To correct for the phase difference in the interferogram between the HeNe laser observations and the 630.0 nm emission, we fit the average Doppler shift measured when looking at the HeNe laser to the average Doppler shift measured while observing to the zenith direction. Unlike the method of strictly using the zenith observations as our zero reference, which forces the vertical wind to be zero at all times, fitting the average laser Doppler to the average zenith Doppler only forces the average vertical wind to be zero. The horizontal wind is obtained from the resulting absolute line-of-sight wind by correcting for the zenith angle of the observations.

[13] The method in which zonal and meridional winds are inferred from the FPI data is based on the observing mode implemented by the two FPI systems. When the two FPI stations are operating independently from one another, each FPI makes measurements toward the zenith followed by the sequential observations in the four cardinal directions—north, east, south, and west—at a zenith angle of 45°. After these images are obtained, a laser calibration image is taken. This cardinal mode sequence has a cadence of ~27 min. For the present study, only the zonal wind data obtained from the east look direction from Merihill, which lies close to the geomagnetic equator, are used when the FPIs were operating in this mode. This mode is the default mode when only one of the two stations was operational.

[14] When both FPI observatories in Peru are operational, they can operate in an alternate observing mode in which bistatic measurements are made in the same common volume regions of the thermosphere in the east (CVE) and west (CVW) look directions. These common volume measurement points are measured at a zenith angle of approximately 51°, and the locations of these points CVE (12.48°S, 74.35°W) and CVW (14.42°S, 77.42°W) are shown in Figure 1. The two FPI stations look simultaneously at the common volume points, which are chosen such that the line-of-sight look directions from the two stations are orthogonal to each other in the horizontal plane at the common volume point. This allows the simultaneous measurements from the two stations to be analyzed such that a horizontal wind vector (comprised of both the meridional and zonal winds) at the common volume point can be estimated. Because this estimate relies on simultaneously analyzing the measurements from the two sites, clear skies are required at both stations. We have used the CVE measurement for the analysis presented here whenever this measurement is available, as this point is located near the geomagnetic equator approximately 3° east of viewing volume of the Jicamarca ISR.

[15] Regardless of the operating mode used to collect the data, estimates of the neutral winds have been culled to remove periods of cloud cover, which obscure the airglow layer from being observed from the ground. The differences in the zonal winds measured in the geographic coordinate system from the geomagnetic directions are negligible since both locations are very close to the geomagnetic equator,

Table 1. Summary of Measurements of FPI Winds, PICASSO EPBs, and ISR Plasma Drifts During March 2011 to March 2012

Month	Wind	EPB	Plasma	Wind_EPB	Wind_Plasma	Wind_EPB_Plasma
Mar–Dec 2011	161	57	29	26	26	2
Jan–Mar 2012	83	42	-	37	-	-
Total	244	99	29	63	26	2

The data are grouped by operational mode used for the neutral wind measurements: CV mode (March to December 2011) and cardinal mode (January to March 2012).

which has a very small declination (~1°). Therefore, the zonal neutral winds estimated from both modes are directly used to compare with the EPB velocities and plasma drifts velocities along the geomagnetic direction.

2.2. EPB Velocity Measurements

[16] We use the PICASSO imaging system for measuring the OI 630.0 nm nightglow emissions to derive the zonal drift velocity of EPBs. PICASSO uses a custom optical design used to image the 630.0 nm emission onto a 2184 × 1472 pixel CCD. The field of view of this particular PICASSO instrument is approximately 80° × 60°, covering approximately 18° of geomagnetic latitude at an assumed emission altitude of 250 km. The spatial resolution is ~0.5 km at the center and ~1.0 km at the edges of the field of view. The CCD is cooled to at least −30°C to reduce the noise contributions from dark current. The exposure time is 90 s for each image, and dark images are recorded frequently to remove noise and read-out biases [for details, see *Makela and Miller*, 2008].

[17] The PICASSO narrow-field imager is deployed at Cerro Tololo Inter-American Observatory, Chile. The imager is oriented equatorward in such a way that its optical axis is almost parallel to the geomagnetic field lines in the *F*-region, as suggested by *Tinsley* [1982]. This orientation is favorable as individual lines of sight from the imaging system are nearly parallel to the geomagnetic field lines through the emission layer, allowing for detailed imaging of EPB structure, which are elongated along the magnetic field lines. The field of view of PICASSO projected into the geographic coordinates at an assumed altitude of 250 km is shown in Figure 1 by the dark region (like a flat cone). In the plot, dash-dot lines (cyan color) denote the apex altitudes within the field of view, ranging from ~300 to 600 km. The horizontal dash lines in the map indicate the geomagnetic latitudes (10°S and 15°S), whereas the vertical dash lines are the geomagnetic longitudes drawn to show the field lines crossing through the field of view of the imager over the geomagnetic equator.

[18] We utilize the OI 630.0 nm airglow images collected by the PICASSO imager from CTIO to estimate EPB velocities using a method similar to that described by *Yao and Makela* [2007]. In order to calculate the EPB velocity, the individual images are first spatially registered using the star field. The stars are then removed from the images using a point suppression methodology. The images are then projected into geographic coordinates assuming an airglow emission altitude of 250 km. A Keogram representation of the sequence of images obtained on a given night is produced by taking slices through the images along a line of constant geomagnetic latitude centered on the same geomagnetic longitude of the FPI measurements being used to estimate the neutral winds (i.e., at the same longitudes of the CVE point at a geomagnetic latitude of ~8.5°S). The average intensity of the images as a function of local time is removed from the Keogram plot. The velocity of an EPB is then estimated by correlating the intensities of consecutive slices in the Keogram plot and dividing the longitudinal offset of plasma depletion features calculated from the lag of the maximum correlation by the time interval between slices. Additional details of this method for estimation of the EPB velocity have been described by *Chapagain et al*. [2012a].

[19] It is important to note that the airglow emission layer is typically distributed over the range of ~225–275 km. However, in processing the OI 630 nm airglow image, we assume a centroid altitude of 250 km and the uncertainty in the measurements of EPB velocity at this altitude from the correlation technique described above is ±4 m/s. In addition, due to variations in the altitude of the emission layer (by 50 km), the calculated velocity can change by approximately ±1 m/s. Both of these uncertainties are taken into consideration in our analysis in addition to the variation of the drift velocity calculation for the average value within the time bin of 30 minutes.

2.3. Plasma Drift Measurements

[20] We use incoherent scatter radar observations made at the Jicamarca Radio Observatory in Peru to derive the equatorial zonal plasma drifts in the *F*-region ionosphere. The basic procedure for the *F*-region plasma drifts measurements has been described by *Kudeki et al.* [1999]. In brief, the radar consists of a large 50 MHz antenna split into two beams pointed about 2.5° to the east and 4.3° to the west of vertical and perpendicular to the geomagnetic field. The line-of-sight drifts obtained in each look direction are combined to give the vertical and zonal plasma drift components. Altitudinal resolution of the measurement is ~15 km with time integration of 5 min. The data used in this study are obtained from averaging over the altitude range of 225–270 km, corresponding to the assumed altitude range of the 630.0 nm airglow emission layer.

3. Results

[21] Table 1 summarizes the coincident observations of the neutral winds by FPI measurements in Peru (either cardinal mode east from MRH or CVE observations from both MRH and NZK), OI 630.0 nm airglow image measurements by the PICASSO imager at CTIO, Chile, and ambient plasma drifts obtained from ISR observations from Jicamarca, Peru. The data are obtained over a 1 year period from March 2011 to March 2012 and are grouped by the neutral wind measurement technique used to collect the data: common volume mode (March to December 2011)

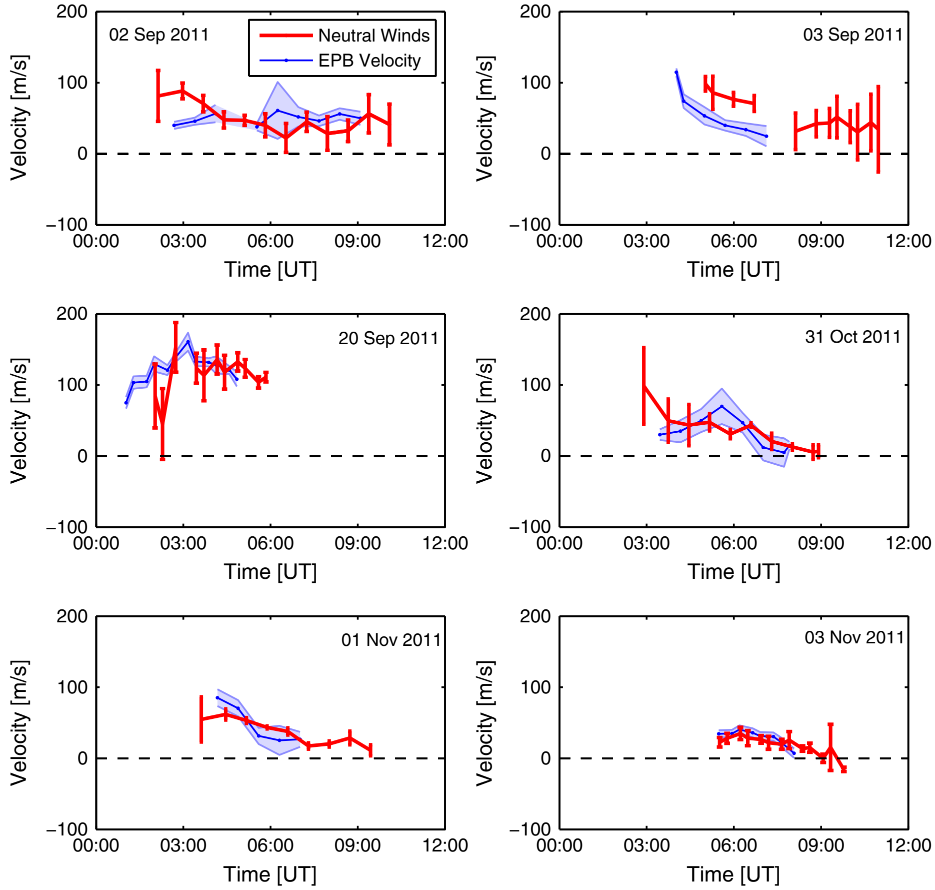

Figure 2. Comparison of the zonal neutral wind speeds with EPB velocities (eastward positive) during the period of simultaneous observations on six nights from September to November 2011. All days are geomagnetically quiet ($\sum Kp < 18$) with solar flux index ($F_{10.7}$ cm) between ~100 and 140.

or cardinal mode (January to March 2012). We have included the total number of observations recorded for neutral winds measurements (244 nights), EPB measurements (99 nights), and the ambient plasma drifts observations (29 nights). Coincident measurements of the neutral winds and EPB velocities were obtained on 63 nights, while coincident wind and ISR plasma drift measurements were obtained on 26 nights. Only two nights have simultaneous observations of the winds, EPB, and plasma drifts. It is important to note that the EPB velocity estimates require the presence of EPBs in the imager's field of view and thus are mainly available during the typical "spread-*F* season," September through April for western South America [*Sobral et al.*, 2002; *Hysell* and *Burcham*, 2002]. However, the ISR plasma drift measurements have no such restriction, although drifts cannot be measured from regions in which coherent scatter caused by spread-*F* is present.

[22] The FPI winds measurements obtained in 2011 were made using the common volume observing mode, while the data from 2012 were analyzed using the cardinal mode from Merihill as described above. In this study, we select six nights of data from the September to November period from 2011 and four nights from February to March 2012 for detailed analysis of simultaneous observations of neutral winds and EPBs. We also present eight nights of data from June, August, and September 2011 for the coincident measurements of FPI neutral winds with the plasma drift velocity from ISR observations. These selected nights are representative of the overall trends of measurements obtained during the observation period. The observations analyzed in this study were made in solar moderate conditions ($80 < F_{10.7} < 140$) and most often geomagnetically quiet days. Because the local times in Chile (LT = UT – 4) and Peru (LT = UT – 5) are different, we present our analysis in terms of universal time.

3.1. Comparisons Between Winds and EPB Velocities

[23] The results of the zonal neutral winds measured using the common volume mode and EPB drifts velocities for six nights selected from September to November 2011 are shown in Figure 2. All data presented in this plot correspond to times of quiet geomagnetic conditions ($\sum Kp < 18$, sum of 3 h Kp value during 24 h period). The EPB velocity was estimated from the PICASSO images for structures centered along the geomagnetic meridian of the CVE point used for the neutral wind measurements. However, the EPB velocity is estimated at higher latitudes (closer to the center of the imager's field of view), corresponding to an apex altitude of ~400 km. The results presented here for the EPB velocities were averaged into 30 min bins, corresponding to the neutral wind time bins. In the plots presented here, positive values correspond to eastward motion. The measurement

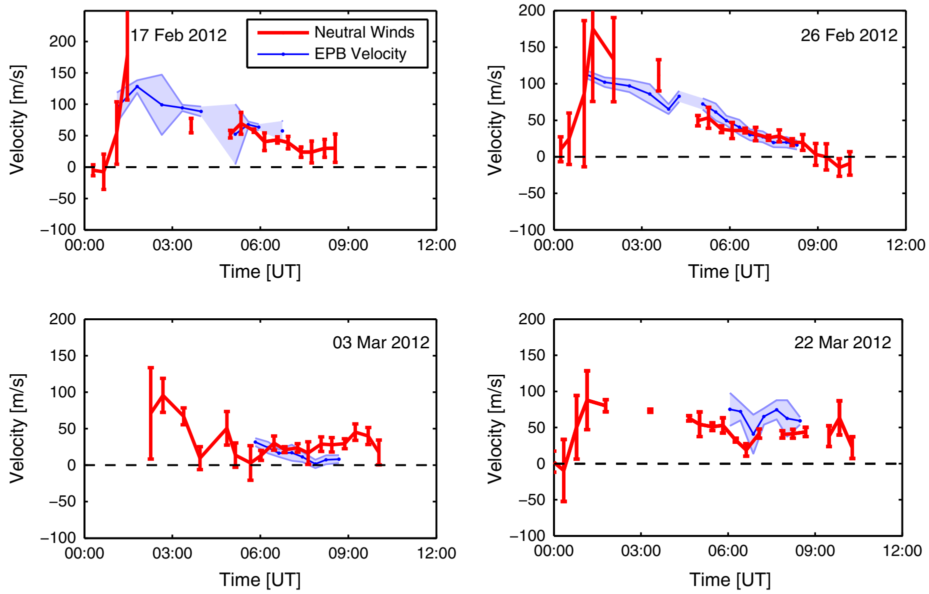

Figure 3. Same as Figure 2 but during February to March 2012. All days are geomagnetically quiet ($\sum Kp < 18$) with solar flux index ($F_{10.7}$ cm) between ~90 and 123.

uncertainties for the wind speeds indicated by the vertical bars are determined by the analysis routine and represent the statistical uncertainty in the fit of the observed data [*Makela et al.*, 2011]. The main controlling factor of this uncertainty is the 630.0 nm airglow emission intensity. Before local midnight, this uncertainty is typically 10 m/s, increasing after local midnight to ~10 – 20 m/s as the intensity of the emission decreases, although periods with larger uncertainties do occur. The uncertainly in the measurements of the EPB velocity is represented by the shaded region around the velocity plot (blue lines).

[24] Figure 3 presents the comparison of the coincident measurements of zonal neutral winds with the EPB zonal drift velocities on four representative nights from February to March 2012. All plots correspond to geomagnetically quiet conditions ($\sum Kp < 18$). During this period, the neutral wind measurements were obtained using the cardinal mode in the east look direction from Merihill. In this mode, we estimated the EPB velocity using bubbles centered along the same geomagnetic meridian of the FPI east wind measurement location, shown in Figure 1. The results illustrate generally good agreement between the winds and the EPB velocities. In most cases, as in Figure 2, the discrepancies between the measurements lie within the uncertainties of the measurements, illustrating that the temporal variations of the neutral winds and EPB velocities are, essentially, the same.

[25] These results also illustrate an early evening increase in the motion of both the ionosphere and thermosphere at ~01:00 UT (21:00 LT at Chile and 20:00 LT at Peru), thereafter generally decreasing during the rest of the night. EPB velocities are not available in the early evening hour during the most of the nights as the EPB structures are not seen in the PICASSO images in the early evening hours. However, the presented data illustrate that the EPB velocities show similar behavior to the neutral winds later in the evening. For example, results show that during most of the nights, the peak values of both neutral winds and EPB velocities do not exceed 100 m/s. However, there are cases, on 20 September 2011 for example, in which the peak zonal speeds of both neutral winds and EPBs exceed 150 m/s. Hence, the changes in magnitude of the neutral winds and EPB velocities are consistent from night to night, indicating that these velocities are highly correlated with each other.

[26] Although the general trends and magnitudes of the winds and EPB velocities are comparable on most nights, on some occasions, there are discrepancies between the wind and EPB velocity. For example in Figure 2, during some occasions on 02 September (at ~06:00 UT), 20 September (at ~02:00 UT), 31 October (at ~05:00 UT), and 01 November (at ~04:00 UT) 2011, the average EPB velocity is larger than the neutral winds. While on some other occasions on 02 September (at ~03:00 UT), 03 September (at ~04:00–06:00 UT), and 20 September (at ~02:00 UT) 2011, the magnitude of the neutral winds is greater than that of the EPB velocity.

[27] The histogram plots in Figure 4 summarize the differences between the neutral winds and EPB velocities, while the line plot represents the total number of events as a function of time for all nights of coincident observations. The data are binned for each hour between 02:00 UT and 09:00 UT. For this plot, 43 nights of coincident observations during July to December 2011 and January to March 2012 are used. The results presented here do not include data from all 63 nights of coincident observations of neutral winds and EPB velocities as shown in Table 1 due to insufficient data available for the computation of differences on some nights. For each hour, the differences between winds and EPB velocities are binned in three ranges: less than −20 m/s, −20 to 20 m/s, and greater than 20 m/s. Here, negative values for the difference (less than −20 m/s) correspond to the EPB velocity being larger than the neutral winds, while the positive values (>20 m/s) represents winds larger than EPB velocities. The range of value −20 to 20 m/s is considered to represent the neutral winds being the same as the EPB velocities since this range lies within the typical value of uncertainties in the measurements.

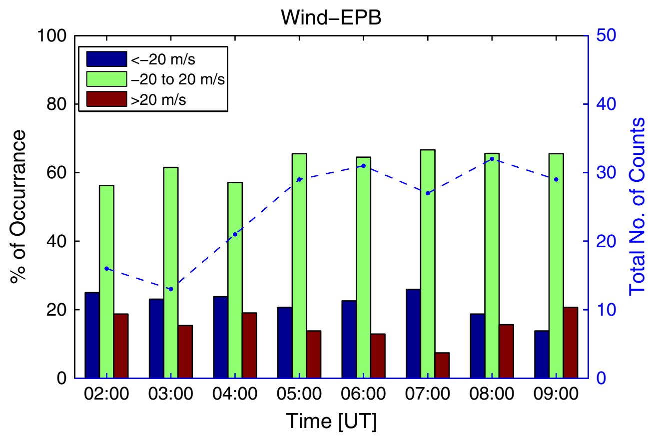

Figure 4. Histograms showing the percent occurrence of the difference between the zonal neutral wind speeds and EPB velocities binned by hour. The line plot indicates the total number of events considered in each hourly bin. The differences of less than −20 m/s represent the EPB velocity faster than neutral winds, >20 m/s represent the wind speeds larger than EPB velocities, and −20 to 20 m/s indicate EPB velocity being the same as the neutral winds.

[28] The results in Figure 4 show that for 55–70% of total events, the neutral winds and EPB velocities are observed to be the same (−20 to 20 m/s bins). However, for ~7–20% of the total events, the magnitude of the neutral winds speeds are observed to be greater than that of the EPB velocity (>20 m/s bins). Interestingly, a considerable percentage of events (~15–25%) shows EPB velocities larger than the neutral winds (less than −20 m/s bins). This is unexpected since the *F*-region dynamo is driven by the neutral winds. The plasma velocity, therefore, is not expected to exceed the wind velocity. As discussed below, this observation is possibly due to the fact that the bubble velocity measurements presented here correspond to a higher apex altitude (~400 km) than the altitude of the neutral wind measurements (~250 km).

4.2. Comparisons Between Winds and Plasma Drifts

[29] Figure 5 shows eight representative nights of comparison between the FPI neutral winds and the ISR plasma drift velocities selected from June, August, and September 2011. All plots correspond to geomagnetically quiet conditions ($\sum Kp < 18$) except for 07 August 2011 ($\sum Kp = 30$). The neutral winds obtained from the CVE mode and plasma drifts estimates correspond to the same altitude (~250 km) and latitude but at a longitudinal difference of about 2.5° (275 km). The average plasma drift velocities are averaged into 30 min bins.

[30] The results presented in Figure 5 reveal similar patterns in the zonal neutral winds and plasma drift velocities with an excellent agreement during most nights. Similar to the results seen in the previous section (Figures 2 and 3), both the winds and plasma drift velocities increase in the early evening hours, attaining peak values of ~100 m/s on most nights. The plasma drift velocities decrease around and after local midnight, falling to nearly zero around the dawn hours and sometimes reversing in the early morning. Occasionally, the observations show discrepancies between the neutral wind speeds and plasma drift velocities. However, these discrepancies overlap within the uncertainties in the measurements (errors bars) of the neutral winds and plasma drift velocities except for a few data points (e.g., 8 June, 3 August, and 5 August) illustrating that the variation of the zonal drift velocities of the plasma is consistent with the background neutral winds.

[31] Figure 6 presents the differences between neutral winds and the plasma drift velocities throughout the observation period summarized in histograms and line plots, constructed in a manner similar to that used to create Figure 4, above. This figure shows that ~60–80% of the events exhibit good agreement between winds and drift velocities (in the range of −20 to 20 m/s bins) and such consistency increases from early evening hours (~60%) through the post-midnight period (~80%). However, we note that we have a limited number of observations, as indicated by the line plot, especially in the early evening hours (8–10 nights during 02:00–05:00 UT), to draw conclusions from.

[32] The number of cases with the plasma drifts exceeding the neutral winds (i.e., less than −20 m/s bins) comprise up to 15% of total events in each bin, while the number of events with the neutral winds greater than the plasma drifts (>20 m/s bins) varies between 5% to 33%, with a maximum in the early evening hours (~02:00 UT–04:00 UT), decreasing through the post-midnight period with minimum value in the early morning hours (~08:00–09:00 UT).

4.3. Comparisons of Winds, EPB Velocities, and Plasma Drifts

[33] Figure 7 shows comparisons of the zonal neutral winds with coincident measurements of EPB velocities (shaded blue region) and the ambient plasma drift velocities. We only have two nights on which all three datasets are available: 04 and 09 August 2011. Note that the region from which the EPB velocities are obtained is slightly to the east of the location measured by either the FPIs or the Jicamarca ISR, so the estimates of velocities and winds are not exactly collocated.

[34] In the top panel of Figure 7, the shaded region during ~01:30–04:30 UT represents a period of strong equatorial spread-*F* in the range time intensity (RTI) plot recorded by the Jicamarca ISR. In regions exhibiting spread-*F*, the radar returns are dominated by coherent, rather than incoherent, scatter and plasma drifts are not inferred. Regions not affected by the presence of spread-*F* can still provide drift measurements. However, during this time, the amount of data involved in the average across altitudes is reduced due to the presence of the spread-*F*, and so the ISR drift estimates during these times are not as robust as during periods devoid of spread-*F*. After ~04:30 UT, the ESF signature over Jicamarca disappears and the plasma drift motion is recorded. Thereafter, the plasma drifts match the neutral winds and EPB velocity, observed from Chile, as well.

[35] During the night of 09 August 2011 (bottom panel of Figure 7), the signature of equatorial spread-*F* over the radar is thin and the plasma drift velocities are measured throughout the night. The results illustrate that the neutral winds and EPB velocities show consistent behavior with the ambient plasma drift velocities. Unfortunately, on these nights, the useable data for the neutral winds and EPB velocities

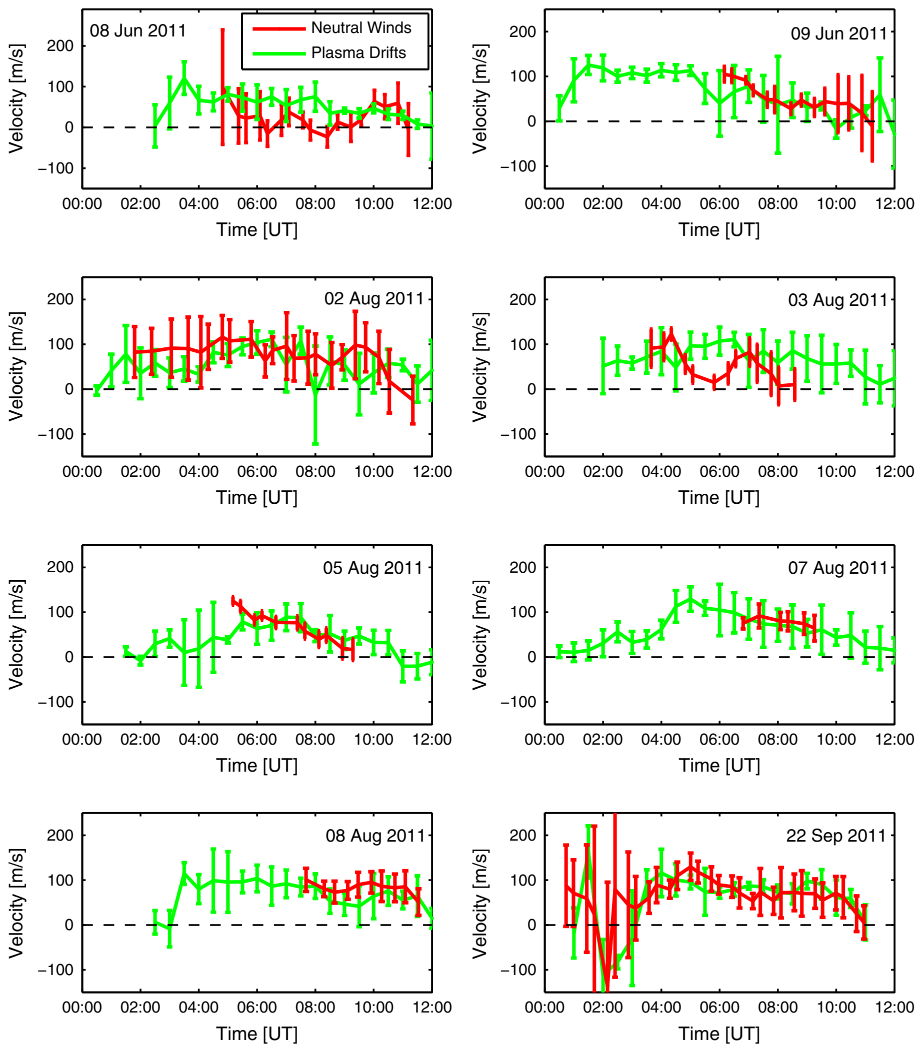

Figure 5. Comparison between zonal neutral winds and plasma drift velocities during periods of simultaneous measurements for eight nights selected from June, August, and September 2011. All days are geomagnetically quiet ($\sum Kp < 18$) except on 07 August ($\sum Kp = 30$) with solar flux index ($F_{10.7}$ cm) between ~80 and 130.

measurements were available only for a short period as shown in the figure.

[36] The results presented above clearly illustrate a good match between the nighttime variations of the zonal neutral winds, the EPB velocities, and the plasma drifts. This reveals that the *F*-region dynamo is highly activated and that the EPB velocity represents the background motions in the *F*-region. However, we do not have sufficient coincident observations available to draw this conclusion during the early evening hours.

5. Discussion

[37] The coincident observations obtained from the 1 year period from March 2011 to March 2012 in western South America reveal good agreement between the FPI zonal neutral winds, optical imaging EPB velocities, and ISR plasma drifts. The results exhibit interesting features with similar patterns of nighttime and night-to-night variations of the neutral winds, EPB, and plasma drift velocities. The magnitude of the change in neutral winds compares favorably to the change in EPB velocities and the plasma drifts. The increase in the early evening eastward speeds of the zonal neutral winds related to the day-to-night pressure gradient most often peaks at ~100 m/s. This is most likely due to the reduced ion drag caused by the decrease in plasma density in the lower thermosphere in the early evening due to the recombination of the *F*-region ionosphere as well as the uplift of the *F*-layer to higher altitudes driven by the development of the pre-reversal enhancement in the electric field.

[38] The EPB velocities, plasma drifts, and neutral winds show a great deal of day-to-day variability, as seen in the plots. The zonal velocities of the EPBs in the off-equatorial region measured from Chile and neutral winds observed near the geomagnetic equator over Peru both decrease to a minimum value (occasionally to zero) after midnight, remaining small into the early morning hours. The time sequences of both EPB velocities and plasma drifts exhibit excellent agreement similar to previous studies of the nighttime zonal motion of

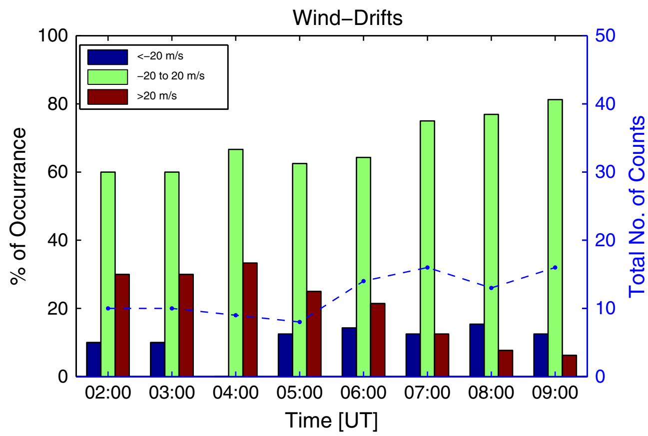

Figure 6. Same as Figure 4 but for the difference between zonal neutral wind speeds and ambient plasma drift velocities.

the equatorial ionosphere-thermosphere system such as the study of *Fejer et al*. [2005], which presented a climatological study of plasma drift velocity using long-term incoherent scatter radar observations from Jicamarca, Peru. However, only a few studies of the zonal neutral wind, EPB, and plasma drifts in the equatorial *F*-region have been performed on a one-to-one basis. For example, *Valladares et al*. [2002] reported similar behaviors in the zonal scintillation drift speeds derived from a spaced-receiver technique and the coincident zonal neutral winds measured by the FPI at Arequipa, Peru. Their results showed occasions in which the wind and drift differed significantly but that the two were primarily consistent, similar to our findings.

[39] Similar to what we have observed in this study, the recent study by *Chapagain et al*. [2012a] shows an excellent agreement between the zonal neutral winds and EPB velocity (mainly after ~21:00 LT) using an extensive dataset of coincident observations of EPB and neutral winds from the low-latitude region of northeastern Brazil. They suggested that the drift velocity of the large-scale plasma depletion structures (i.e., EPBs) observed off the geomagnetic equator represents the background plasma motion. However, shortly after sunset (~19:00 LT), the EPB zonal velocity was smaller than that of the neutral winds on many nights, illustrating that the *F*-region dynamo is not fully activated during the period in which the EPB is undergoing significant growth and development. In our present study, we do not have enough events of observations in the early evening hours (before ~21:00 LT) to draw a similar conclusion for the western South American sector. Nevertheless, the available data show that the nighttime variations of the neutral winds (after 02:00 UT or 21:00 LT) reveal similar trends to that of the EPB velocities or plasma drifts on most of the nights. In our results, excellent quantitative agreement between the ISR plasma drifts and FPI neutral winds is found on up to 80% of total observations (Figure 6). A similar behavior was reported in the comparisons of the diurnal variations of the Jicamarca ISR plasma drifts with the zonal neutral winds determined by the DE-2 satellite observations [*Fejer et al*., 1985; *Herrero and Mayr*, 1986].

[40] Interestingly, the present observations show examples of differences in the magnitude of the EPB velocities or plasma drifts compared to the background neutral winds on several occasions. These differences can be attributed to two causes: (1) the measurements of neutral winds, EPB, and plasma drifts which are not exactly collocated and (2) vertical polarization electric fields created inside of the EPBs.

[41] The results summarized in Figure 4 show that the average EPB velocities measured from Chile are significantly larger than that of the neutral winds on up to ~25% of the nights of observations. The EPB velocity estimates were made at higher latitudes (~1000 km south from the neutral winds measurements) corresponding to an apex altitude of about ~400 km, while the altitude of the line-of-sight averaged Doppler shift measured by the FPI is located within the bottom side of the *F*-layer at an altitude of 250 km, which is the assumed centroid of the 630.0 nm airglow emission. Thus, the wind measurements are coming from the bottom side of the *F*-layer, while the EPB velocity estimates are coming from a region geomagnetically connected to the equatorial *F*-layer. Therefore, an altitudinal gradient in the velocity profile at the geomagnetic equator could cause the differences in the magnitude of the EPB velocity (measured off of the geomagnetic equator) and the winds (measured at the magnetic equator). This finding is supported by *Chapagain et al*. [2012b] who used optical imaging data from Ascension Island to investigate the latitudinal shear of the EPB velocity. They reported latitudinal (altitudinal) shears in the EPB velocity of up to 0.12 m/s/km, with higher speeds corresponding to higher latitudes (higher apex altitudes). This would also be consistent with the "backwards C-shape" observed in radar and satellite measurements [*Woodman and LaHoz*, 1976; *Kelley et al*., 2003] resulting from an altitudinal shear in the eastward plasma flow velocity, which peaks near the *F* peak at the equator and decreases both above and below that height.

[42] Similarly, previous studies of the zonal neutral winds

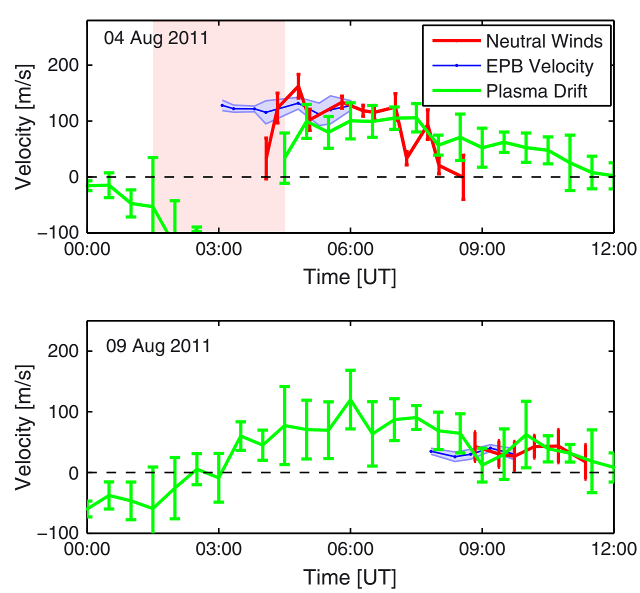

Figure 7. Comparisons of zonal neutral winds, EPB velocities, and the plasma drifts for simultaneous observing periods. The days are geomagnetically quiet ($\sum Kp$ = 5, 14) with solar flux index ($F_{10.7}$ cm) of 111 and 94.

using CHAMP and DE-2 observations [*Liu et al.*, 2009] and simulations with the NCAR TIEGCM model [*Kondo et al.*, 2011] have reported the detection of a fast wind jet at the Earth's dip equator (at ~400 km altitude) instead of the geographic equator, demonstrating the strong geomagnetic control of the neutral dynamics via ion drag. Furthermore, *Miyoshi et al.* [2012] have illustrated an altitudinal shear of the zonal neutral winds from numerical simulation of the equatorial wind in the thermosphere. They indicated that the magnitude of the nighttime zonal neutral winds exhibits a relatively higher value at 400 km altitude compared to that from 200 km, which is consistent with our results of EPB velocity (measured off of the geomagnetic equator) at times being larger than the neutral winds.

[43] The differences in the wind-EPB velocity could also be due to a substantial polarization electric field that can be created inside a large EPB near its walls [e.g., *Huang et al.*, 2010], which makes the EPB velocities somewhat different than that of the background plasma drifts or neutral winds. As explained above, it must be noted that the volumes probed by the PICASSO, ISR, and the FPI are not exactly collocated. Therefore, we cannot completely rule out the effect of the vertical polarization electric fields for the differences in relative velocities between the EPB and neutral winds.

[44] Similarly, wind-plasma drift speed differences can be explained by the presence of horizontal (latitude and longitude) gradients in both the ISR plasma drifts and the FPI neutral winds as measurements do not correspond to exactly collocated common volume regions. The measurements from neutral winds are separated by about 250 km and 280 km in longitude for the cardinal east look direction and CVE mode, respectively, and tens of km in latitude from the ISR plasma drift observations. In addition, as suggested by *Anderson and Mendillo* [1983] and *Anderson et al.* [1987], the wind motion could be more localized depending on the thermospheric tides, heat sources, and the interaction with the local ionosphere, while the plasma drift is mainly influenced by the field line integrated conductivity.

[45] A smaller plasma drift speed as compared to the neutral wind speeds (in our work, up to 33% of total events) might be caused by the persistence of non-negligible *E*-region conductivity after sunset, which can partially short out the polarization electric field in the *F*-region. On the other hand, occasionally, a higher plasma drift speed as compared with the neutral wind is seen that might be caused by an additional polarization electric field generated by an altitude gradient of the zonal neutral wind as explained by the previous studies conducted by *Coley et al.* [1994] using the DE-2 satellite observations, *Valladares et al.* [2002] from the correlative study of the zonal neutral winds and scintillation drifts measurements, and *Huang et al.* [2010] using satellite observations.

6. Conclusions

[46] We have used a 1 year dataset obtained in the western South American sector from March 2011 to March 2012 to study the relationship between nighttime thermospheric zonal neutral winds, EPB velocities, and ionospheric plasma drifts. The results illustrate that the nighttime temporal variations of the zonal velocities of EPBs and plasma drifts correlate well with the zonal neutral winds. The nighttime eastward winds, EPB velocities, and plasma drifts increase in the early evening hours, attaining peak values of ~100 m/s on most of the nights, before decreasing to a minimum value in the local midnight and post-midnight periods. In addition to similar patterns of nighttime variations, the night-to-night variations of the zonal winds, EPB velocities, and plasma drifts are generally consistent with each other. Similarly, the magnitudes of the zonal velocities of the neutral winds, EPBs, and plasma drifts often show good agreement illustrating that the *F*-region dynamo is generally fully activated.

[47] However, on several occasions, the EPB velocities are found to be faster than the neutral winds. We believe that this difference in relative velocities is caused either by the polarization electric field created inside the EPB or an altitudinal gradient of the neutral winds and EPB velocity measurements. On some other nights, the neutral wind speeds exceed the speeds of the EPB or plasma drifts. However, a detailed study based upon a larger database needs to be carried out before a final conclusion can be reached.

[48] Of interest for future study will be the continued collection of a long-term database which can be used to examine the change in behavior of the *F*-region dynamo with the change in the phase of the solar cycle between solar minimum and solar maximum. Coordinated multi-instrument experiments using direct comparisons of simultaneous observations rather than relying on monthly averages or climatological comparisons of neutral winds, plasma drifts, and EPB velocities provide a significant opportunity to enhance our understanding of the day-to-day variability in the development of the *F*-region dynamo and how this ion-neutral thermospheric-ionospheric coupling changes throughout the solar cycle. Such simultaneous observing allows the removal of the masking of the forcing functions underlying the development of night-to-night variability created by the averaging process inherent in the production of these climatologies, and the details of the underlying physical processes may be more clearly examined.

[49] **Acknowledgments.** N. P. Chapagain was supported by the NASA Living With a Star Heliophysics Postdoctoral Fellowship Program, administered by the University Corporation for Atmospheric Research (UCAR). Work at the University of Illinois at Urbana-Champaign and Clemson University was supported by National Science Foundation CEDAR grants ATM-0940253 and ATM-0940217, respectively. The Jicamarca Radio Observatory is a facility of the Instituto Geofisico del Peru operated with support from the NSF AGS-0905448 through Cornell University. We thank the Jicamarca staff, and in particular O. Veliz and L. Navarro, for helping with the operations and measurements of the Fabry-Perot interferometers.

References

Anderson, D. N., and M. Mendillo (1983), Ionospheric conditions affecting the evolution of equatorial plasma depletions, *Geophys. Res. Lett.*, *10*, 541.

Anderson, D. N., R. A. Heelis, and J. P. McClure (1987), Calculated night-time eastward plasma drift velocities at low latitudes and their solar cycle dependence, *Ann. Geophys. Ser. A.*, *5*, 435.

Basu, S., S. Basu, E. Kudeki, H. P. Zengingonul, M. A. Biondi, and J. W. Meriwether (1991), Zonal irregularity drifts and neutral winds measured near the geomagnetic equator in Peru, *J. Atmos. Terr. Phys.*, *53*, 743.

Basu, S. et al. (1996), Scintillations, plasma drifts, and neutral winds in the equatorial ionosphere after sunset, *J. Geophys. Res.*, *101*, 26,795.

Biondi, M. A., J. W. Meriwether, B. G. Fejer, and R. Woodman (1988), Measurements of the dynamics and coupling of the equatorial thermosphere and the F-region ionosphere in Peru, *J. Atmos. Terr. Phys.*, *50*, 937.

Biondi, M. A., J. W. Jr.Meriwether, B. G. Fejer, S. A. Gonzalez, and D. C. Hallenbeck (1991), Equatorial thermospheric wind changes during the solar cycle: Measurements at Arequipa, Peru, from 1983 to 1990, *J. Geophys. Res.*, *96*, 15,917–15,930, doi:10.1029/91JA01645.

Chapagain, N. P., M. J. Taylor, and J. V. Eccles (2011), Airglow observations and modeling of *F* region depletion zonal velocities over Christmas Island, *J. Geophys. Res.*, *116*, A02301, doi:10.1029/2010JA015958.

Chapagain, N. P., J. J. Makela, J. W. Meriwether, D. Fisher, R. A. Buriti, and A. F. Medeiros (2012a), Comparison of nighttime zonal neutral winds and equatorial plasma bubble drift velocities over Brazil, *J. Geophys. Res.*, *117*, A06309, doi:10.1029/2012JA017620.

Chapagain, N. P., M. J. Taylor, J. J. Makela, and T. M. Duly (2012b), Equatorial plasma bubble zonal velocity using 630.0 nm airglow observations and plasma drift modeling over Ascension Island, *J. Geophys. Res.*, *117*, A06316, doi:10.1029/2012JA017750.

Coley, W. R., and R. A. Heelis (1989), Low-latitude zonal and vertical ion drifts seen by DE-2, *J. Geophys. Res.*, *94*, 6751–6761.

Coley, W. R., R. A. Heelis, and N. W. Spencer (1994), Comparison of low-latitude ion and neutral zonal drifts using DE-2 data, *J. Geophys. Res.*, *99*, 341–348, doi:10.1029/93JA02205.

Fejer, B. G., E. Kudeki, and D. T. Farley (1985), Equatorial *F* region zonal plasma drifts, *J. Geophys. Res.*, *90*, 12,249–12,255, doi:10.1029/JA090iA12p12249–12,255, doi:10.1029/JA090iA12p12249.

Fejer, B. G., J. R. Souza, A. S. Santos, and A. E. Costa Pereira (2005), Climatology of *F* region zonal plasma drifts over Jicamarca, *J. Geophys. Res.*, *110*, A12310, doi:10.1029/2005JA011324.

Heelis, R. A., P. C. Kendall, R. J. Moffet, D. W. Windle, and H. Rishbeth (1974), Electrical coupling of the *E* and *F* regions and its effect on the *F* region drifts and winds, *Planet. Space Sci.*, *22*, 743–756.

Herrero, F. A., and H. G. Mayr (1986), Tidal decomposition of zonal neutral and ion flows in the Earth's upper equatorial thermosphere, *Geophys. Res. Lett.*, *13*, 359.

Huang, C.-S., O. de La Beaujardiere, R. F. Pfaff, J. M. Retterer, P. A. Roddy, D. E. Hunton, Y. -J. Su, S.-Y. Su, and F. J. Rich (2010), Zonal drift of plasma particles inside equatorial plasma bubbles and its relation to the zonal drift of the bubble structure, *J. Geophys. Res.*, *115*, A07316, doi:10.1029/2010JA015324.

Hysell, D. L., and J. D. Burcham (2002), Long term studies of equatorial spread *F* using the JULIA radar at Jicamarca, *J. Atmos. Sol. Terr. Phys.*, *64*, 1531–1543, doi:10.1016/S1364-6826(02)00091-3.

Immel, T. J., H. U. Frey, S. B. Mende, and E. Sagawa (2004), Global observations of the zonal drifts speed of equatorial ionospheric plasma bubbles, *Ann. Geophys.*, *22*, 3099–3107, doi:10.5194/angeo-22-3099-2004.

Kelley, M. C. (1989), *The Earth's Ionosphere: Plasma Physics and Electrodynamics*, *43*, pp. 71–129, Academic Press, San Diego, California.

Kelley, M. C., J. J. Makela, L. J. Paxton, F. Kamalabadi, J. M. Comberiate, and H. Kil (2003), The first coordinated ground- and space-based optical observations of equatorial plasma bubbles, *Geophys. Res. Lett.*, *30*, 1766, doi:10.1029/2003GL017301.

Kondo, T., A. D. Richmond, H. Liu, J. Lei, and S. Watanabe (2011), On the formation of a fast thermospheric zonal wind at the magnetic dip equator, *Geophys. Res. Lett.*, *38*, L10101, doi:10.1029/2011GL047255.

Kudeki, E., and S. Bhattacharyya (1999), Postsunset vortex in equatorial *F* region plasma drifts and implications for bottomside spread F, *J. Geophys. Res.*, *104*, 28,163–28,170.

Kudeki, E., S. Bhattacharyya, and R. F. Woodman (1999), A new approach in incoherent scatter F region ExB drift measurements at Jicamarca, *J. Geophys. Res.*, *104*, 28145–28162.

Link, R., and L. L. Cogger (1988), A reexamination of the O I 6300-Å nightglow, *J. Geophys. Res.*, *93*, 9883–9892, doi:10.1029/JA093iA09p09883.

Liu H., S. Watanabe, and T. Kondo (2009), Fast thermospheric wind jet at the Earth's dip equator. *Geophys. Res. Lett.*, *36*,L08103, doi:10.1029/2009037377.

Makela, J. J., and E. S. Miller (2008), Optical observations of the growth and day-to-day variability of equatorial plasma bubbles, *J. Geophys. Res.*, *113*, A03307, doi:10.1029/2007JA012661.

Makela, J. J., J. W. Meriwether, Y. Huang, and P. J. Sherwood (2011), Simulation and analysis of a multi-order imaging Fabry-Perot interferometer for the study of thermospheric winds and temperatures, *Appl. Opt.*, *50*, 4403, doi:10.1364/AO.50.004403.

Makela, J. J., D. J. Fisher, J. W. Meriwether, R. A. Buriti, and A. F. Medeiros (2013), Near-continual ground-based nighttime observations of thermospheric neutral winds and temperatures over northeastern Brazil from 2009–2012, *J. Atmos. Sol.-Terr. Phys.*, doi:10.1016/j.jastp.2012.11.019.

Martinis, C., J. Meriwether, R. Niciejewski, M. Biondi, C. Fesen, and M. Mendillo (2001), Zonal neutral winds at equatorial and low latitudes, *J. Atmos. Sol. Terr. Phys.*, *63*, 1559–1569, doi:10.1016/S1364-6826(01)00022-0.

Martinis, C., J. V. Eccles, J. Baumgardner, J. Manzano, and M. Mendillo (2003), Latitude dependence of zonal plasma drifts obtained from dual site airglow observations, *J. Geophys. Res.*, *108*(A3), 1129, doi:10.1029/2002JA009462.

Mendillo, M., and J. Baumgardner (1982), Airglow characteristics of equatorial plasma depletions, *J. Geophys. Res.*, *87*, 7641–7652.

Meriwether, J. W. Jr., J. W. Moody, M. A. Biondi, and R. G. Roble (1986), Optical interferometric measurements of nighttime equatorial thermospheric winds at Arequipa, Peru, *J. Geophys. Res.*, *91*, 5557–5566, doi:10.1029/JA091iA05p05557.

Meriwether, J. W., J. J. Makela, Y. Huang, D. J. Fisher, R. A. Buriti, A. F. Medeiros, and H. Takahashi (2011), Climatology of the nighttime equatorial thermospheric winds and temperatures over Brazil near solar minimum, *J. Geophys. Res.*,*116*, A04322, doi:10.1029/2011JA016477.

Miyoshi, Y., H. Fujiwara, H. Jin, H. Shinagawa, and H. Liu (2012), Numerical simulation of the equatorial wind jet in the thermosphere, *J. Geophys. Res.*, *117*, A03309, doi:10.1029/2011JA017373.

Rishbeth, H. (1971), Polarization fields produced by winds in the equatorial *F* region, *Planet. Space Sci.*, *19*, 357–369.

Sobral, J. H. A., M. A. Abdu, H. Takahashi, M. J. Taylor, E. R. de Paula, C. J. Zamlutti, and G. L. Borba (2002), A study of the ionospheric plasma bubbles climatology over Brazil, based on 22 years (1977–1998) of OI 630 nm airglow observation, *J. Atmos. Sol. Terr. Phys.*, *64* (12–14), 1517–1524, doi:10.1016/S1364-6826(02)00089-5.

Sobral, J. H. A., et al. (2009), Ionospheric zonal velocities at conjugate points over Brazil during the COPEX campaign: Experimental observations and theoretical validations, *J. Geophys. Res.*, *114*, A04309, doi:10.1029/2008JA013896.

Tinsley, B. A. (1982), Field aligned airglow observations of transequatorial bubbles in the tropical F region, *J. Atmos. Terr. Phys.*, *44*, 547–557.

Valladares, C., R. Sheehan, S. Basu, H. Kuenzler, and J. Espinoza (1996), The multi-instrumented studies of equatorial thermosphere aeronomy scintillation system: Climatology of zonal drifts, *J. Geophys. Res.*, *101*(A12), 26839–26850.

Valladares, C. E., J. W. Meriwether, R. Sheehan, and M. A. Biondi (2002), Correlative study of neutral winds and scintillation drifts measured near the magnetic equator, *J. Geophys. Res.*, *107*(A7), 1112, doi:10.1029/2001JA000042.

Wharton, L. E., N. W. Spencer, and H. C. Mayr (1984), The Earth's thermospheric superrotation from Dynamics Explorer 2, *Geophys. Res. Lett.*, *11*, 531.

Woodman, R. F. (1972), East-west ionospheric drifts at the magnetic equator, *Space Res.*, *81*, 5447–5466.

Woodman, R. F., and C. LaHoz (1976), Radar observations of F-region equatorial irregularities, *J. Geophys. Res.*, *81*, 5447–5466.

Yao, D., and J. J. Makela (2007), Analysis of equatorial plasma bubble zonal drift velocities in the pacific sector by imaging techniques, *Ann. Geophys.*, *25*, 701–709, doi:10.5194/angeo-25-701-2007.